HOLOGIC®
The Science of Sure

Powerful images.
Clear answers.

Manage Patient's concerns about Atypical Femur Fracture*

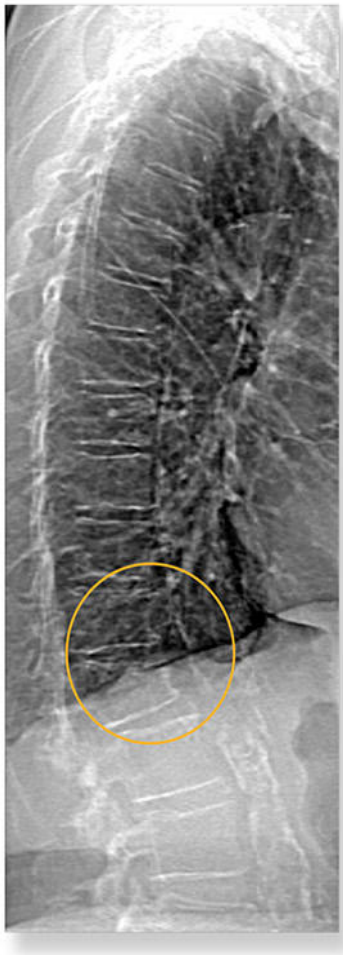

Vertebral Fracture Assessment – a critical part of a complete fracture risk assessment

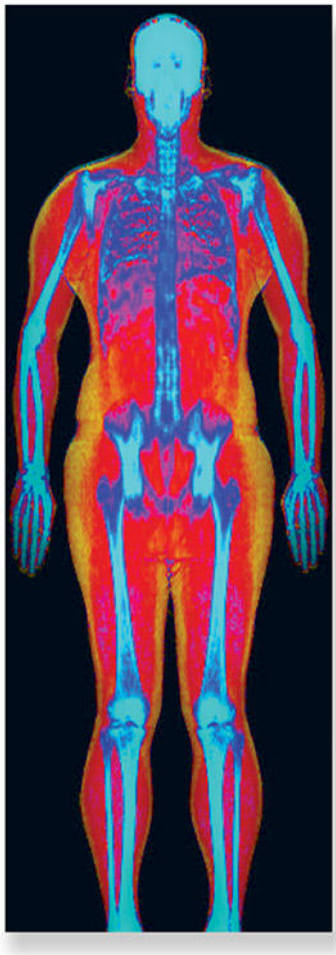

Advanced Body Composition® Assessment – the power to see what's inside

Contact your Hologic rep today at insidesales@hologic.com

*Incomplete Atypical Femur Fractures imaged with a Hologic densitometer, courtesy of Prof. Cheung, University of Toronto

www.hologic.com | info@hologic.com | 1.781.999.7300

A rare mutation in *SMAD9* associated with high bone mass identifies the SMAD-dependent BMP signalling pathway as a potential anabolic target for osteoporosis

Celia L Gregson (PhD, FRCP), [1]* Dylan Bergen (PhD), [1,2]† Paul Leo (PhD), [3]† Richard B. Sessions (PhD), [4] Lawrie Wheeler (BSc), [3] April Hartley (BSc), [1,5] Scott Youlten (PhD), [6] Peter I Croucher (PhD), [6,7,8] Aideen M. McInerney-Leo (PhD), [9,3] William Fraser (MD), [10,11] Jonathan C.Y. Tang (MSc), [10] Lisa Anderson (B.BiomedSci), [3] Mhairi Marshall (MSc), [3] Leon Sergot (FRCR), [12] Lavinia Paternoster (PhD), [5] George Davey-Smith (MD), [5] The AOGC Consortium, [3] Matthew A Brown (MD, FRACP), [3] Chrissy Hammond (PhD), [2] John P Kemp (PhD), [13,5] Jon H Tobias (FRCP), [1]+ Emma L Duncan (PhD), [14,3,15] +

1. Musculoskeletal Research Unit, Translational Health Sciences, Bristol Medical School, University of Bristol, Bristol, UK
2. School of Physiology, Pharmacology, and Neuroscience, Faculty of Life Sciences, University of Bristol, Bristol, UK
3. Translational Genomics Group, Institute of Health and Biomedical Innovation, Faculty of Health, Queensland University of Technology (QUT), Translational Research Institute, Princess Alexandra Hospital, Ipswich Rd, Woolloongabba, QLD 4102, Australia.
4. School of Biochemistry, Faculty of Life Sciences, University of Bristol, Bristol, UK
5. Medical Research Council Integrative Epidemiology Unit, Population Health Sciences, Bristol Medical School, University of Bristol, Bristol, BS8 2BN, UK
6. Division of Bone Biology, Garvan Institute of Medical Research, Sydney, NSW 2010, Australia
7. St Vincent's Clinical School, Faculty of Medicine, UNSW Sydney, Sydney NSW 2010, Australia

This article has been accepted for publication and undergone full peer review but has not been through the copyediting, typesetting, pagination and proofreading process which may lead to differences between this version and the Version of Record. Please cite this article as doi: 10.1002/jbmr.3875

8. School of Biotechnology and Biomolecular Sciences, UNSW Sydney, Sydney, NSW 2052, Australia
9. Dermatology Research Centre, The University of Queensland, The University of Queensland Diamantina Institute, Brisbane, Queensland, Australia.
10. Norwich Medical School, University of East Anglia, Norwich Research Park, Norwich, NR4 7TJ, UK.
11. Departments of Diabetes, Endocrinology and Clinical Biochemistry, Norfolk and Norwich University Hospital NHS Foundation Trust, Colney Lane, Norwich, UK
12. Severn School of Radiology, Severn Deanery, Park House, Bristol, BS34 8YU, UK
13. The University of Queensland Diamantina Institute, The University of Queensland, Woolloongabba, QLD 4102, Australia.
14. Department of Endocrinology and Diabetes, Royal Brisbane & Women's Hospital, Butterfield St, Herston, QLD 4029, Australia.
15. Faculty of Medicine, University of Queensland, Herston, QLD 4006, Australia.

† These authors contributed equally to this work.

+ These authors contributed equally to this work

***Corresponding author:** Dr Celia L Gregson, Musculoskeletal Research Unit, Translational Health Sciences, Bristol Medical School, University of Bristol, Learning & Research Building (Level 1), Southmead Hospital, Bristol, BS10 5NB, UK. Tel: 0044 117 4147842.

Email: celia.gregson@bristol.ac.uk

Supplementary data are included with this submission

Disclosures: The authors declare that no competing interests exist.

Keywords: High Bone Mass; *SMAD9*; DXA; exon sequencing; monogenic; zebrafish; osteoanabolic

Abstract

Novel anabolic drug targets are needed to treat osteoporosis. Having established a large national cohort with unexplained high bone mass (HBM), we aimed to identify a novel monogenic cause of HBM and provide insight into a regulatory pathway potentially amenable to therapeutic intervention. We investigated a pedigree with unexplained HBM in whom previous sequencing had excluded known causes of monogenic HBM. Whole exome sequencing identified a rare (minor allele frequency 0.0023), highly evolutionarily conserved, missense mutation in *SMAD9* (c.65T>C, p.Leu22Pro) segregating with HBM in this autosomal dominant family. The same mutation was identified in another two unrelated individuals both with HBM. *In-silico* protein modelling predicts the mutation severely disrupts the MH1 DNA-binding domain of SMAD9. Affected individuals have bone mineral density [BMD] Z-Scores +3 to +5, mandible enlargement, a broad frame, torus palatinus/ mandibularis, pes planus, increased shoe size and a tendency to sink when swimming. Peripheral quantitative computer tomography (pQCT) measurement demonstrates increased trabecular volumetric BMD and increased cortical thickness conferring greater predicted bone strength; bone turnover markers are low/normal. Notably, fractures and nerve compression are not seen. Both genome-wide, and gene-based association testing involving estimated-BMD measured at the heel in 362,924 white British subjects from the UK Biobank Study showed strong associations with *SMAD9* (P_{GWAS} = 6 x 10^{-16}; P_{GENE} = 8 × 10^{-17}). Furthermore, we found Smad9 to be highly expressed in both murine cortical bone derived osteocytes and skeletal elements of zebrafish larvae. Our findings support *SMAD9* as a novel HBM gene, and a potential novel osteoanabolic target for osteoporosis therapeutics. SMAD9

is thought to inhibit bone morphogenetic protein (BMP) dependent target gene transcription to reduce osteoblast activity. Thus, we hypothesise *SMAD9* c.65T>C is a loss-of-function mutation reducing BMP inhibition. Lowering *SMAD9* as a potential novel anabolic mechanism for osteoporosis therapeutics warrants further investigation.

Introduction

Age-related bone loss with deterioration of skeletal architecture leads to osteoporosis, affecting 8.2 million women and 2.0 million men aged 50 years and older in the United States (US) (1). Worldwide, osteoporosis causes more than 8.9 million fractures annually (1). Osteoporotic fractures and their treatment are a major cause of morbidity and mortality, with annual US healthcare costs exceeding $20 billion (2). Most osteoporosis treatment approaches, including all oral medications, reduce bone resorption and prevent further bone loss, rather than enhance bone formation. Affordable anabolic treatments, which can restore bone mass and skeletal architecture, are much needed.

Romosozumab, a monoclonal antibody against sclerostin, represents a new class of anti-osteoporosis drug, recently approved by the FDA (3, 4). Sclerostin, a key inhibitor of bone formation, was discovered through study of two rare syndromes of extreme high bone mass (HBM) due to mutations in *SOST* (5, 6). *SOST* encodes Sclerostin, which binds to low-density lipoprotein receptor-related proteins 5 and 6 (LRP5 and LRP6) to prevent activation of canonical WNT signalling in bone, resulting in decreased bone formation. Gain-of-function mutations in *LRP5* and *LRP6* can also cause extreme HBM (7, 8). Together these

sclerosing bone dysplasias are characterised by mandible enlargement with tori of the palate and mandible, bone overgrowth leading to nerve compression, a tendency to sink when swimming, and, importantly, resistance to fracture (5, 7, 9). These important gene discoveries validate the study of rare monogenic HBM as an approach to identify novel therapeutic targets for drug development towards osteoporosis treatments.

We have previously shown that HBM (defined as a total hip and/or first lumbar vertebral bone mineral density [BMD] Z-score of ≥ +3.2) is observed in 0.18% of Dual-Energy X-ray Absorptiometry (DXA) scans in the UK (10). Most cases are unexplained, *i.e.* they do not carry mutations in established HBM genes (9). Whilst such HBM populations do show enrichment for common variant associations with established BMD-associated loci (11), we hypothesized that novel causes of monogenic HBM remain to be determined. Thus, we aimed to identify novel monogenic causes of HBM to provide insight into regulatory pathways amenable to therapeutic intervention.

Materials and Methods

The UK HBM Cohort

The HBM study is a UK-based multi-centered observational study of adults with unexplained HBM, identified incidentally on routine clinical Dual-energy X-ray absorptiometry (DXA) scanning. Full details of DXA database screening and participant recruitment have been reported (10) (Supplemental Methods). In brief, DXA databases containing 335,115 DXA scans across 13 UK centers were searched; all scans explained by artefact of known causes of

high BMD were excluded. Unexplained HBM was defined as a) first Lumbar Vertebra (L1) Z-score of ≥ +3.2 plus Total Hip (TH) Z-score of ≥ +1.2 and/or b) TH Z-score ≥ +3.2 plus L1 Z-score of ≥ +1.2. 533 unexplained HBM cases were invited to participate; 248 (47%) were recruited. They passed on study invitations to first-degree relatives and spouse/partner(s). 236 of 893 (26.4%) of invited relatives were recruited, as were 61 of 217 (28.1%) of invited spouses/ partners (10). All participants underwent structured clinical assessment and DXA scanning (Supplemental Methods). Peripheral Quantitative Computed Tomography (pQCT) scans were performed at the distal and mid-shaft of the tibia (4 & 66% from distal endplate) in the non-dominant lower limb using a Stratec XCT2000L (Stratec Medizintechnik, Germany) as published previously (12) (Supplemental Methods). Two non-fasted EDTA samples were collected and serum separated and frozen within 4 hours to -80°C. Bone formation (Procollagen type 1 amino-terminal propeptide [P1NP], total osteocalcin) and resorption (β-C-telopeptides of type I collagen [βCTX]) markers and sclerostin were measured (Supplemental Methods). DNA was extracted from peripheral venous blood using standard phenol/ chloroform extraction. Sanger sequencing of all HBM index cases for exons 2, 3 and 4 of *LRP5*, *SOST* (including the van Buchem disease deletion) and *LRP4* (exons 25 and 26) excluded seven with *LRP5* mutations and one with a *SOST* mutation, leaving 240 unexplained HBM individuals (9).

Anglo-Australasian Osteoporosis Genetics Consortium (AOGC) HBM and LBM cases

The original AOGC extreme truncate population included 1128 Australian, 74 New Zealand and 753 British women, aged 55–85 years, ≥5 years postmenopausal, with either HBM (age and gender-adjusted TH BMD Z-scores +1.5 to +4.0, n=1055) or low bone mass (LBM) (Z-

scores -4.0 to -1.5, n=900) (13). LBM cases were excluded if they had secondary causes of osteoporosis (as previously described (13)). Unrelated samples of Caucasian ancestry with complete height and weight data and enough high-quality genomic DNA were available in 947 individuals (426 AOGC high and 521 AOGC low BMD), from which (computation capacity limited sample size) the most extreme HBM cases were selected using a threshold TH or LS Z-score ≥+2.5, and the most extreme LBM cases using a LS Z-Score ≤-0.5, so 126 HBM and 493 LBM samples were chosen to undergo whole exome sequencing (WES).

Whole exome sequencing

Sequencing libraries for 859 samples (240 UK HBM, 126 AOGC HBM, and 493 AOGC LBM) were constructed. Base calling, sequence alignment and variant calling were performed as previously described (14) (details in Supplemental Methods).

Filtering pipeline applied to unexplained HBM pedigrees

After quality-filtering, data were analyzed for carriage of at least one rare (either novel or maximum population-based minor allele frequency (MAF) <0.005) nonsynonymous SNV or indel in a highly conserved region (GERP score <1.5) of a gene, carried by the affected individuals and not carried by unaffected individuals (*i.e.* autosomal dominant carriage model). Data were then filtered based on functional prediction of SNVs using Polyphen (15) to identify 'probably damaging' and SIFT (16) 'deleterious' SNVs. Compound heterozygous and homozygous inheritance were also assessed.

Sanger sequencing validation of pedigree based HBM mutation

Polymerase chain reaction (PCR) amplification of identified exons was performed on 50ng genomic DNA (see Supplemental Methods 4). Electropherograms were aligned and analysed using sequence analysis software Genalys (Version 2.0 ß, Masazumi Takahashi).

Multi-marker Analysis of GenoMic Annotation (MAGMA) in UK Biobank

Gene-based tests of association were performed on 362,924 unrelated white British subjects (54% female) from the UK Biobank study with ultrasound derived heel estimated BMD (eBMD) and high-quality genome-wide HRC and 1000G/UK10K imputed data (Supplemental Methods). Detailed methodology has been published (17). Gene-based tests of association were implemented in MAGMA v1.06 (18) using a multi-model approach combining association results from three separate gene analysis models: principal components regression, SNP-wise Mean $\chi 2$ model [*i.e.* test statistic derived as sum of -log(SNP p-value)] and SNP-wise Top $\chi 2$ model [(test statistic derived as sum of -log(SNP p-value) for top SNPs)] to produce an aggregate p-value corresponding to the association between each of the 19,361 protein coding genes (+/- 20kb) and BMD, adjusting for age, sex, genotyping array, assessment center and 20 ancestry informative principal components, with gene-based significance threshold ($p<2.87x10^{-6}$) (17).

Phenome-wide association study (PheWAS)

PheWAS was conducted using GWASATLAS (https://atlas.ctglab.nl/) an online database of publicly available summary results statistics from 4,155 GWAS from 295 unique studies across 2,960 unique traits and 27 domains (19). Significance for pleiotropic associations used a traditional genome-wide significance threshold for SNP-trait PheWAS ($p< 5x10^{-8}$) (17).

Gene expression in murine osteocytes

Whole transcriptome sequencing data from the primary osteocytes of four different bone types (tibia, femur, humerus and calvaria) from mice (marrow removed, n=8 per bone) were analysed. A threshold of expression was determined based on the distribution of normalised gene expression for each sample (20). "Expressed" genes were those exceeding this threshold for all 8 of 8 replicates in any bone type. Osteocyte enriched expression of these genes in the skeleton was determined by comparing transcriptome-sequencing data from bone-samples with osteocytes isolated versus those samples with marrow left intact (n=5 per group) (21).

Replication in high BMD populations

WES data from AOGC were analysed to identify any individual who carried the same rare (MAF <0.025) mutation as identified from analysis of the HBM pedigree. Polyphen (15) and SIFT (16), PMut (22) and MutationTaster (23) were used for *in silico* functional prediction. When the same point mutation was identified in more than one individual, haplotypes were compared between index case samples genotyped using an Infinium OmniExpress-12v1.0 GWAS chip read using an Illumina iScan (San Diego, California, USA), with genotype clustering performed using Illumina BeadStudio software.

Protein structural modelling

The amino-acid sequence of human SMAD9 was passed to the HHPred server (24). This located the best template structures in the Protein Databank for the MH1 domain, 5X6G (mouse SMAD5; 92% identity), and the MH2 domain, 3GMJ (*Drosophila melanogaster* MAD; 75% identity). Modeller was used to build the domain models according to the HHPred alignments (25). Chimera was used to introduce point mutations and remodel the domain swapping in the SMAD9-MH1 model (26).

Zebrafish studies

BMPre:GFP (*Tg(5xBMPRE-Xla.Id3:GFP)*) (27) and *sp7:GFP* (*Tg(Ola.sp7:NLS-GFP)*) (28) transgenic fish (in London AB background) were housed and maintained in standard conditions (29, 30). Experiments were approved by the University of Bristol Animal Welfare and Ethical Review Body (AWERB) and performed in accordance with a UK Home Office project license. Developmentally staged larvae (following euthanization in MS222) were fixed in 4% paraformaldehyde (1 hour), dehydrated to 100% methanol and stored at -20°C prior to staining. Immunolabelling was as previously described (31). Primary antibodies: anti-Smad9 (rabbit polyclonal, Abcam, ab96698) used at a 1/100 dilution and anti-GFP (chicken polyclonal, Abcam, ab13970) used at a 1/200 dilution in blocking buffer (5% horse serum). Secondary antibodies were used (A21206 and A11041, Invitrogen) in a 1/400 dilution and samples incubated with DAPI (Sigma-Aldrich, 1/1000 dilution) to visualise nuclei. Samples were mounted in 1% low melting point agarose and imaged with a confocal laser scanning microscope (Leica, SP5II AOBS attached to a Leica DM I6000 inverted epifluorescence microscope) using a 40X PL APO CS (1.3 numerical aperture) lens. Images were processed and colour balanced in Fiji (32).

Results

HBM pedigree with a segregating *SMAD9* c.65T>C p.Leu22Pro variant (Fig 1 and Table 1)

We investigated a pedigree with unexplained and apparently autosomal dominant HBM (9), identified from our large UK HBM cohort (10) (Fig. 1).

Clinical phenotype (Table 1)

Clinical phenotypes of the UK family individuals are shown in Table 1; extended clinical histories are provided in S1 Results. In summary, affected individuals had high BMD Z-scores, and very high body mass index (BMI); and had not had any adult fractures, nerve compression or dental problems; however, bone pain was common, without a clear cause. There was no clinical history of intellectual impairment, pulmonary hypertension, vascular hypertension, haematological abnormalities, pubertal delay or other clinical conditions. None had been exposed to anabolic or antiresorptive medications.

III.1: Index Case (c.65T>C, p.Leu22Pro)

The 33-year-old index case, with BMD Z-Scores +3.2 at the total hip and +4.5 at first lumbar vertebra (L1), had only sustained one traumatic fracture aged 20 months. She reported lower leg and ankle pain. She was tall (>97th centile) and obese, with increased shoe size, a broad frame, enlarged mandible and a 4mm torus mandibularis. She had normal joints. Radiographs showed increased cortical thickness and new bone formation at the anterior inferior iliac spines bilaterally (Supplemental Fig. 1).

II.2: Mother of the index case (c.65T>C, p.Leu22Pro)

The 55-year-old affected mother, with BMD Z-Scores +3.3 at the total hip and at L1, had never sustained a fracture. Six years earlier she had had a right calcaneal spur surgically removed. She had widespread pain with a diagnosis of fibromyalgia. She was tall (97th centile) and obese, with above average shoe size, a broad frame, enlarged mandible but no tori. She had a full range of movement in all joints, bilateral knee crepitus and bilateral pes planus.

III.2: Half-sister to index case (c.65T>C, p.Leu22Pro)

The 22-year-old affected half-sister, with BMD Z-Scores +4.8 at the total hip and +2.6 at L1, had not fractured. She had had sciatica for five years, lumbar back pain and fronto-temporal headaches for 11 years, with a diagnosis of migraine. She was tall (93rd centile) and obese, with above average shoe size, a broad frame, enlarged mandible, a torus palatinus in the midline of her hard palate (3cm x 7mm) and normal joint movement.

I.2: Grandmother of index case (wild-type)

The 75-years-old grandmother, who did not have HBM, had also never sustained a fracture. She had widespread osteoarthritis and on examination had reduced extension of the right elbow and left knee, and bilateral knee crepitus. However, in contrast to other family members, she was less overweight with normal shoe size, frame, mandible and no tori.

Sequencing of pedigree

WES identified a heterozygous missense variant in *SMAD9 (SMAD family Member 9 referring to homologies to the Caenorhabditis elegans SMA (small worm phenotype) and Drosophila MAD ("Mothers Against Decapentaplegic"))* (NM 001127217: exon2: c.65T>C, p.Leu22Pro), segregating with HBM (*i.e.* present in all three individuals with HBM (*III.1, II.2, III.2*), but absent from *I.2* (Fig. 1). This variant (rs111748421) is rare (Exome Aggregation Consortium [ExAC] minor allele frequency [MAF] 0.0023 in European non-Finnish populations), affects a highly evolutionarily conserved base (genomic evolutionary rate profiling [GERP] 5.53) and is predicted to be pathogenic by multiple protein-prediction algorithms (deleterious by SIFT (16), probably damaging by Polyphen (15), and disease causing by MutationTaster (23) and PMut (22)).

A novel variant in *CHRNA1 (cholinergic receptor, nicotinic, alpha 1)* (c.560T>C, p.Leu187Pro) was also identified (GERP 5.29). Mutations in *CHRNA1* have been associated with congenital myasthenic syndromes (OMIM#100690), not present in this pedigree. No variants were identified when applying a compound heterozygous or an autosomal recessive inheritance model.

Sequencing of other HBM cases identifies two further isolated HBM cases harbouring a c.65T>C**, p.Leu22Pro variant**

WES of a further 366 HBM cases (240 isolated cases from the UK cohort with a total hip (TH) or L1 Z-score ≥+3.2 and 126 individuals from the Anglo-Australasian Osteoporosis Genetics Consortium (AOGC) (33) with either a total hip and/or lumbar spine (LS) Z-score between +2.5 and +4.0) (Supplemental Fig. 2) identified two individuals with the same *SMAD9* c.65T>C, p.Leu22Pro variant. Haplotypic analysis confirmed these women were neither related to each other nor to the pedigree described above.

Clinical phenotype

Isolated HBM case (c.65T>C, p.Leu22Pro) from the UK (Table 1; Supplemental Fig. 3 and Results 1). This 55-year-old female, with BMD Z-Scores +5.0 at the total hip and +4.7 at L1, had never fractured and had no symptoms of nerve compression. Her adult left upper cuspid tooth had never erupted; wisdom teeth had been extracted for overcrowding. She had noticed her own mandible enlargement. She had a congenital astigmatism of her left eye with poor vision, and congenital bilateral pes planus. Height was normal (30^{th} centile). She was obese with a broad frame, mandible enlargement, but no tori. She had normal joints.

Isolated HBM case (c.65T>C, p.Leu22Pro) from Australia

This 57-year-old female, with BMD Z-Scores +3.0. at the total hip and +2.7 at L1, reported a nose fracture as a child. Height was on the 45th centile and she was overweight. She did not have any history of conditions affecting bone health; and had not received antiresorptive or anabolic medications. No further clinical details were available.

Tibial pQCT evaluation

All members of the HBM pedigree, plus the additional isolated HBM case from the UK underwent pQCT scanning of the tibia (Table 2, Supplemental Table 1 and Supplemental Fig. 4). To set these findings in context, the mean (SD) values from the four c.65T>C, p.Leu22Pro *SMAD9* HBM cases were compared against values from 76 unrelated female HBM cases (without *SMAD9, LRP5, LRP4, or SOST* mutations) and 32 female family controls with normal DXA-measured BMD who had had pQCT scans following the same protocol (12). The four *SMAD9* HBM cases had greater trabecular density, cortical area and thickness and predicted bone strength (strength stain index [SSI]) than other HBM cases, and, to a greater extent, than unaffected family controls. Muscle size (cross-sectional area) was also notably larger in the *SMAD9* HBM group (Table 2).

Sequencing of Low Bone Mass (LBM) cases

WES data from 473 women with LBM from the AOGC consortium with TH Z-scores between -1.5 and -4.0 and a LS Z-score ≤-0.5, obtained using similar methodology to the AOGC HBM cases, was interrogated (Supplemental Fig. 2). The c.65T>C, p.Leu22Pro *SMAD9* variant was not observed.

Common *SMAD9*-associated genetic variants and BMD

Publicly available data from a recent population-based genome-wide association study (GWAS) of eBMD (estimated BMD by heel ultrasound in the UK-Biobank study) (17) were used to investigate variants surrounding both *SMAD9* and *CHRNA1*. Regional association plots suggested that SNPs intersecting *SMAD9* are strongly associated with eBMD (lead SNP rs12427846 [MAF 0.25], β 0.02, SE 0.002, $p=5.5x10^{-16}$; Fig. 3). In contrast, SNPs surrounding *CHRNA1* were not robustly associated with eBMD (Supplemental Fig. 5). These observations were further supported by gene-based tests of association performed in-house using 362,924 unrelated white British subjects from the UK-Biobank Study. Specifically, *SMAD9* was more strongly associated with eBMD ($P_{JOINT} = 7.94 \times 10^{-17}$), when compared to neighbouring genes within +/- 800kb ($P > 2.4 \times 10^{-2}$) (Supplemental Table 2). No such enrichment was seen for *CHRNA1* (Supplemental Table 3). Further investigation of rs12427846 in the UK-Biobank Study identified weak associations with body weight (β -0.14, SE 0.04, $p=1.6x10^{-3}$) and with height (β -0.07, SE 0.03, $p=3.5x10^{-3}$) with effects in the opposite direction from that seen with eBMD; however, adjustment for weight and height did not attenuate the strong association between rs12427846 and eBMD reported above. Interrogating the GWAS Catalog (https://www.ebi.ac.uk/gwas/) did not identify associations of the rare (MAF 0.0014) variant rs111748421 with any trait (neither bone-related nor any other).

Phenome-wide association study

PheWAS involving nearly 3000 traits (19) identified no clear evidence for pleiotropy for the c.65T>C, p.Leu22Pro *SMAD9* variant (rs111748421) (Supplemental Fig. 6 and Supplemental Table 4). Analysis involving the common *SMAD9* variant (rs12427846) revealed robust

pleiotropic associations with BMD traits. Similarly, a gene-based PheWAS of *SMAD9*, identified robust evidence of gene-level pleiotropy with BMD To investigate further possible pleiotropic associations with metabolic phenotypes, we looked up rs111748421 and rs12427846 in the Myocardial Infarction Genetics and CARDIoGRAM Exome meta-analysis (34, 35) and the subsequent meta-analysis to which results from UK Biobank SOFT CAD GWAS and CARDIoGRAMplusC4D 1000 Genomes-based GWAS were added (36). No association was seen for rs111748421 in either. Whilst rs12427846 was not present in the first meta-analysis, the eBMD increasing allele was only nominally associated with the composite cardiovascular disease outcome in the second (log OR 0.03 [SE 0.01], $p=9x10^{-4}$; significance threshold $p<5x10^{-8}$) (36).

Smad9 expression in murine osteocytes

We next determined whether *Smad9* and *Chrna1* are expressed in osteocytes, the master cell regulators in the skeleton and key regulators of bone mass (37), and enriched in osteocytes compared to other cells in bone (21). Smad9 mRNA was highly expressed in murine osteocytes whilst Chrna1 was not (Supplemental Table 5).

Smad9 expression in zebrafish skeletal tissue

We also examined Smad9 protein expression in the developing zebrafish skeleton (38) at 6- and 7-days post fertilisation (dpf) (Fig. 3A). A focus of Smad9 expression was observed at the dorsal tip of the opercle, an intramembranous bone overlying the gills, adjacent to but distinct from a region of bone morphogenetic protein (BMP) reporter activity (Fig. 3B). The opercula muscle group also showed evidence of BMP reporter activity, whereas Smad9 expression at this site was absent. Smad9-expressing cells in the opercle were negative for the

osteoblast marker, sp7 (osterix), suggesting they are likely to represent pre-osteoblasts (Fig. 4C and Supplemental Movie 1). Equivalent findings were observed in the branchiostegal ray bones and in the notochord at 6- and 7- dpf (Supplemental Fig. 7).

SMAD9 protein structural modelling

SMAD9 is a TGF-beta family member DNA binding transcription factor. Phosphorylation by BMP-ligand-bound type 1 receptor kinase activates SMAD9, which translocates from the cytoplasm to the nucleus to regulate target gene expression (39). The seven exons of human *SMAD9* encode a protein of 467 amino acids that contains two MAD-homology (MH) domains (MAD: Mother against Dpp) separated by a linker region (Fig. 4). The p.Leu22Pro *SMAD9* mutation is located within the MH1 domain responsible for DNA-binding (Fig. 4), and lies in the hydrophobic face of the N-terminal alpha helix (helix-1) (Fig. 5, Supplemental Movie 2). Helix-1 packs against a groove made by helix-2 and -3 within MH1, forming part of the hydrophobic core of this domain. Substitution of leucine by proline will: a) introduce a less hydrophobic residue into this position; and b) compromise the α-helical fold by disrupting the canonical hydrogen bonding of helix-1. Thus, modelling suggests that this mutation will disrupt the MH1 domain so severely that SMAD9 can no longer bind DNA and/or will be unstable leading to protein degradation.

Discussion

We report the first HBM pedigree with a segregating *SMAD9* mutation, with replication in two further unrelated individuals with HBM. *SMAD9* (also known as *SMAD8, MADH6,* and *MADH9*) encodes a downstream modulator of the BMP signalling pathway. BMPs, members

of the TGF-β superfamily, induce the formation of bone and cartilage (40). SMADs, activated by ligand-binding of cell surface BMP receptors, mediate down-stream intracellular signalling and biological responses induced by BMPs (41). Smad6 and Smad7 both inhibit BMP receptor activation and downstream signalling, as does Smad9 by more direct transcriptional repression (39). Our *in-silico* protein modelling predicts that the p.Leu22Pro mutation severely disrupts the structure of the MH1 DNA binding domain of *SMAD9*, leading to loss-of-function.

Few previous studies have examined sites of Smad9 tissue expression. We have confirmed that Smad9 is expressed in mouse cortical bone derived osteocytes, and the Smad9 protein in skeletal elements of zebrafish larvae. Moreover, we observed that BMP reporter activity in zebrafish was absent at sites of Smad9 expression, consistent with a functional role in BMP repression (39). Mutant mouse models with a *LacZ* insertion causing Smad9 truncation have not undergone BMD phenotyping; however, they have shown strong *LacZ* expression (under control of an endogenous *Smad9* promoter) within developing skeletal sites (e.g. ribs, maxilla, mandible), gut and lungs (42, 43). Taken together our findings suggest that *SMAD9* c.65T>C is a loss-of-function mutation, causing HBM through a novel mechanism of enhanced bone formation due to reduced BMP inhibition.

Further, we have shown that the region containing *SMAD9* is strongly associated with BMD within the general population. Common variants intersecting *SMAD9* associate with population-based measures of eBMD, as evidenced recently by fine-mapping of target genes

(17, 44) and from our gene-based tests of association presented here. Furthermore, rs12427846 [the lead SNP from these eBMD results] is associated with DXA-measured total body BMD (45) and fracture risk (17), also consistent with associations with BMD identified in our PheWAS. These findings provide further evidence of the importance of *SMAD9* in bone biology and are equivalent to reported associations for common variants annotated to *LRP5* and *SOST* genes, both similarly implicated in monogenic HBM disorders (46, 47).

We have previously estimated unexplained HBM to have a prevalence of 0.181% amongst a DXA-scanned adult population in the UK (10). As two of 248 cases fulfilling our stringent HBM phenotype definition (Supplemental Fig. 2) were found to harbour the c.65T>C p.Leu22Pro *SMAD9* variant (rs111748421), we would estimate prevalence of *SMAD9* HBM as approximately 1 in 100,000 (1.46×10^{-5}), less common than *LRP5* HBM (9). As rs111748421 has a reported MAF of 0.0028, this raises the possibility of incomplete penetrance, variable expressivity, gene-gene or gene-environment interaction with a currently unknown factor; it is also possible that rs111748421 might be in linkage disequilibrium (LD) with an intronic regulatory variant not captured by WES.

The clinical phenotype of c.65T>C, p.Leu22Pro *SMAD9* HBM includes mandible enlargement, a broad frame, torus palatinus, pes planus, increased shoe size and, in two of five subjects, a tendency to sink when swimming. Adult fractures were not reported, raising the possibility of increased skeletal strength, supported by evidence of greater cortical bone and an increased strength-strain index (SSI) quantified by pQCT (discussed further below),

both of which promote fracture resistance. Mandible enlargement, torus palatinus, a tendency to sink when swimming, and an absence of adult fractures are reminiscent of *LRP5* HBM (7, 48). Encouragingly, unlike sclerosteosis (due to anabolic *SOST* mutations) and some *LRP5* HBM cases (9, 49), nerve compression was not a feature of *SMAD9* HBM.

The musculoskeletal phenotype of p.Leu22Pro *SMAD9* HBM includes high BMD Z-Scores (+3 to +5), with increased fat and lean mass. Whilst morbid obesity with increased stature were seen in three of five *SMAD9* HBM cases, this was not ubiquitous to all. The increases in BMD of +3.3 to 5 SDs above normal exceeded increases in fat-mass index of +0.9 to 3.4 supporting HBM as the primary phenotype, rather than high BMD occurring as a consequence of high fat mass (50). Furthermore, fat-associated phenotypes were not identified in our PheWAS. pQCT revealed increased volumetric trabecular bone density with greater cortical thickness and area, suggesting reduced bone remodelling to reduce endosteal expansion. In support, bone turnover markers are at the lower end of the normal range. This phenotype mimics that previously described for human *LRP5* HBM (51) although plasma sclerostin is not elevated, in contrast to *LRP5* HBM (52), suggesting that a negative feedback loop downregulating WNT signalling is not present. pQCT further identified larger muscle size in *SMAD9* HBM cases, including in the independent UK case with normal stature. This contrasts with findings from our zebrafish studies that Smad9 expression is absent from skeletal muscle tissue, as is also observed in murine models (43). Given the well-recognised cross-talk between muscle and bone (53) and the large BMI of these individuals, it is conceivable that the increase in muscle size is secondary to a need to carry the substantial

weight of both fat and bone mass. However, similar increases in muscle size have not been reported in other monogenic HBM conditions (*i.e. LRP5* or *SOST* HBM) with equivalent BMD.

A clinical report of 13q13.3-q21.3 deletion, leading to haploinsufficiency of *SMAD9* amongst other genes, identified a phenotype of skeletal overgrowth with infant height >95th percentile, consistent with the adult phenotype we describe, implicating *SMAD9* in the regulation of linear growth (54). We found limited, but consistent, evidence that *SMAD9* HBM may affect longitudinal growth. Whilst differences in height can artefactually affect DXA measured BMD, pQCT measures of increased trabecular bone density and cortical thickness are usually more independent of body size. Heterozygous truncating *SMAD9* mutations are associated with primary pulmonary hypertension (OMIM#615342) (55), a phenotype not apparent in our HBM cases. Reported mutations affect a different domain from the mutation observed here, with p.Cys202X (55) and p.Arg294X (56) truncating the SMAD9 protein in the linker region between MH1 and MH2. A truncating mutation (p.Arg247X) has been associated with cerebral arteriovenous malformations in childhood (57). An activating heterozygous p.Val90Met germline mutation, affecting the 4th α-helix of MH1 and close to the DNA binding interface, has been described in one pedigree with hamartomatous polyposis (58). In contrast to p.Leu22Pro, p.Val90Met appears to be a gain-of-function mutation, thought to arise from a steric clash, prompting a His104 residue to enhance DNA binding (58). Such examples of diverse phenotypes arising from mutations in differing exons of the same gene are well recognised, *e.g.* differing mutations in *FBN1 (Fibrillin 1)* can cause Marfan

syndrome (with associated tall stature) (OMIM#154700), acromicric dysplasias (with short stature) (OMIM#102370), or stiff skin syndrome (OMIM#184900) (59-61).

We are only aware of one other skeletal dysplasia reported in association with an inhibitory SMAD (which include *SMAD6* and *SMAD7*). A rare *SMAD6* mutation has been associated with susceptibility to non-syndromic midline craniosynostosis 7 (OMIM#617439) - but only in the context of co-inheritance of a common variant in *BMP2* strongly associated with this condition, a rare example of two locus inheritance (62). Interestingly, amongst the 1103 conditionally independent SNPs reaching genome-wide significance in the UK-Biobank eBMD GWAS (population n=426,824), as well as identifying the *SMAD9* locus, four novel SNPs annotating to *SMAD7* were reported (plus three established SNPs associated with *SMAD3*), all suggesting variation in inhibitory SMADs is likely of functional importance in human bone biology (17).

The phenotype we describe here contrasts with that of activating mutations of the BMP receptor, *ACVR1*, which increase BMP signalling. However, in contrast to p.Leu22Pro *SMAD9* HBM, *ACVR1* mutations lead to a fatal condition, Fibrous Ossificans Progressiva (FOP, OMIM#135100) (63). In FOP, muscle tissue differentiates into bone following trivial injury, resulting in the formation of mature bone at multiple extra-skeletal sites. *ACVR1* mutations may produce a more severe phenotype, compared with loss-of-function mutations in *SMAD9* reported here, since *ACVR1* also activates non-SMAD-dependent BMP signalling

cascades, such as the NF-κB and p38 MAP kinase (p38MAPK) pathways, which are upregulated in FOP *ACVR1* R206H monocytes (64).

Given the benign phenotype observed in c.65T>C, p.Leu22Pro *SMAD9* carriers, our findings suggest that SMAD9 is worth consideration as a drug target for osteoporosis. Our zebrafish studies suggest that Smad9 is expressed in pre-osteoblasts, consistent with the profile of an anabolic target capable of stimulating new bone formation through recruitment of early osteoblast progenitors. Given the pathological consequence of excess BMP activation in FOP, this pathway has not been prioritised as a possible therapeutic target in osteoporosis, despite the profound bone anabolic potential. Interestingly, phosphorylation of Smad9, as part of the Smad1/5/9 heterotrimer, has been researched in relation to fracture healing and bone regeneration: G-protein-coupled receptor kinase 2-interacting protein-1 (GIT1), a shuttle protein in osteoblasts, regulates Smad1/5/9 phosphorylation, which in turn mediates BMP2 regulation of Runx2 expression and thus endochondral bone formation at fracture sites (65, 66). Moreover, BMP is administered locally to promote bone repair following surgery (67). Based on our findings, it is tempting to speculate that treatments suppressing SMAD9 activity might prove useful in treating osteoporosis, fractures, and possibly also sarcopenia. The potential pleiotropic association between one *SMAD9* variant and a composite cardiovascular phenotype represents the results of life-long exposure to a variant rather than any potential short-term perturbations in a gene pathway as might be exploited therapeutically.

Our study has limitations. All individuals with c.65T>C, p.Leu22Pro *SMAD9* HBM were female, reflecting the study design which favoured those with a historical DXA scan who are

more likely to be female. Whether findings will be similar in men is unknown, although no sex-gene interaction has been described for the *LRP4, LRP5, LRP6,* or *SOST* sclerosing bone dysplasias. In the recent UK-Biobank eBMD GWAS, LD score regression analyses suggested that the genetic architecture influencing male and female eBMD was largely shared with some significant differences between the sexes (rG=0.91, SE=0.012, p<0.001) (17), consistent with earlier epidemiological studies (68). The small sample of *SMAD9* HBM cases (n=4 with pQCT) limited our ability to robustly evaluate associations statistically. The c.65T>C, p.Leu22Pro mutation is a reported SNP carried within the general population (*e.g.* in the UK, an estimated 92,428 people might be expected to carry this mutation). This may be the case, given there is no indication that the phenotype affects reproductive fitness, and HBM will not be overt unless a DXA scan is performed. Our GWAS was based on estimated heel BMD quantified by ultrasound rather than DXA-measured BMD. Estimated heel BMD is not used routinely in clinical practice. However, we have previously demonstrated a strong overlap between genetic loci identified by eBMD GWAS and by DXA-measured BMD GWAS (44).

Conclusions

We report *SMAD9* as a novel HBM-causing gene. The clinical phenotype of c.65T>C, p.Leu22Pro *SMAD9* HBM has many features in common with that of *LRP5* HBM, but lacks the deleterious features which characterise *SOST* HBM (sclerosteosis). As reported for both *LRP5* and *SOST*, we demonstrate that a rare mutation in *SMAD9* is associated with an extreme bone phenotype and that common variation in *SMAD9* affects bone density within

the general population. The role of SMAD9 in bone biology is supported by our finding of high levels of Smad9 expression in murine osteocytes, and in skeletal elements of zebrafish larvae. Smad9 is thought to inhibit BMP signalling to reduce osteoblast activity; thus, we hypothesise *SMAD9* c.65T>C is a loss-of-function mutation reducing BMP inhibition, ultimately leading to enhanced bone formation. Our findings support SMAD9, and its role within the SMAD9-dependent BMP signalling pathway, as a potential novel anabolic target for osteoporosis therapeutics which warrants further investigation.

Acknowledgements

Full acknowledgements are listed in the Supplemental Material, including details of the AOGC Consortium**.** ***Funding.*** CLG was funded by the Wellcome Trust (080280/Z/06/Z), the EU 7th Framework Programme ref 247642 (GEoCoDE), a British Geriatric Society travel grant, and Versus Arthritis (formerly Arthritis Research UK) (grant ref 20000). This study was supported by the NIHR CRN (no. 5163). DB received travel grants from The Harold Hyam Wingate Foundation (DMMTF-180208), and an Elizabeth Blackwell Institute for Health Research (University of Bristol) discipline hopping fellowship via a Wellcome Trust Institutional Strategic Support Grant (204813/Z/16/Z). AH is funded by the Wellcome Trust (20378/Z/16/Z). LP, AH and GDS work in a unit which receives UK Medical Research Council funding (MC_UU_12013/4). CH and DB were funded by Versus Arthritis (21211, 21937, 19476). AML is supported by an NHMRC Early Career Fellowship. JPK is funded by a University of Queensland Development Fellowship (UQFEL1718945) his contribution is supported by a National Health and Medical Research Council (Australia) project grant

(GNT1158758). MAB is supported by an NHMRC Senior Principal Research Fellowship. PIC is funded by a Wellcome Trust Strategic Award (101123). The AOGC was funded by the National Health and Medical Research Council (Australia) (511132 and 1032571). Funders had no role in study design, analysis, or manuscript preparation.

Author Contributions: Conception: CLG, GDS, MAB, JHT, ELD. Design: CLG, JPK, GDS, MAB, PL, JHT, ELD. Data acquisition: CLG, DB, LW, PC, SY, WF, JCYT, CH, MAB, ELD. Analysis: CLG, DB, RBS, LW, AH, SY, PC, AML, CH, JPK, PL, ELD. Interpretation: CLG, DB, RBS, AH, SY, PC, AML, MAB, CH, JPK, PL, JHT, ELD. Manuscript draft: CLG, DB, LW, AH, JPK, LP, CH, JPK, PL, JHT, ELD. Manuscript revision: CLG, DB, RBS, AH, AML, JCYT, LP, MAB, CH, JPK, PL, JHT, ELD. Approve final manuscript – all authors. All authors take responsibility for their contributions as outlined above.

References

1. Wright NC, Looker AC, Saag KG, Curtis JR, Delzell ES, Randall S, et al. The recent prevalence of osteoporosis and low bone mass in the United States based on bone mineral density at the femoral neck or lumbar spine. J Bone Miner Res. 2014;29(11):2520-6.

2. Burge R, Dawson-Hughes B, Solomon DH, Wong JB, King A, Tosteson A. Incidence and economic burden of osteoporosis-related fractures in the United States, 2005-2025. J Bone Miner Res. 2007;22(3):465-75.

3. McClung MR, Grauer A, Boonen S, Bolognese MA, Brown JP, Diez-Perez A, et al. Romosozumab in Postmenopausal Women with Low Bone Mineral Density. New Eng J Med. 2014;370(5):412-20.

4. McClung MR, Brown JP, Diez-Perez A, Resch H, Caminis J, Meisner P, et al. Effects of 24 Months of Treatment With Romosozumab Followed by 12 Months of Denosumab or Placebo in Postmenopausal Women With Low Bone Mineral Density: A Randomized, Double-Blind, Phase 2, Parallel Group Study. J Bone Miner Res. 2018;33(8):1397-406.

5. Brunkow ME, Gardner JC, Van Ness J, Paeper BW, Kovacevich BR, Proll S, et al. Bone Dysplasia Sclerosteosis Results from Loss of the SOST Gene Product, a Novel Cystine Knot-Containing Protein. Am J Med Genet. 2001;68(3):577-89.

6. Staehling-Hampton K, Proll S, Paeper BW, Zhao L, Charmley P, Brown A, et al. A 52-kb deletion in the SOST-MEOX1 intergenic region on 17q12-q21 is associated with van Buchem disease in the Dutch population. Am J Med Genet. 2002;110(2):144-52.

7. Little RD, Carulli JP, Del Mastro RG, Dupuis J, Osborne M, Folz C, et al. A mutation in the LDL receptor-related protein 5 gene results in the autosomal dominant high-bone-mass trait. Am J Hum Genet. 2002;70(1):11-9.

8. Michael P. Whyte, Gary S. Gottesman, Elizabeth L. Lin, William H.Mcalister, Angela Nenninger, Vinieth N. Bijanki, et al., editors. LRP6 Mutation: A New Cause of Autosomal Dominant High Bone Mass. (LB-1172) American Society for Bone and Mineral Research (ASBMR) 2018 Annual Meeting; 2018; Montreal, Canada.

9. Gregson CL, Wheeler L, Hardcastle SA, Appleton LH, Addison KA, Brugmans M, et al. Mutations in Known Monogenic High Bone Mass Loci Only Explain a Small Proportion of High Bone Mass Cases. J Bone Miner Res. 2015;31(3):640-9.

10. Gregson CL, Steel SA, O'Rourke KP, Allan K, Ayuk J, Bhalla A, et al. 'Sink or swim': an evaluation of the clinical characteristics of individuals with high bone mass. Osteo Int. 2012;23(2):643-54.

11. Gregson CL, Newell F, Leo PJ, Clark GR, Paternoster L, Marshall M, et al. Genome-wide association study of extreme high bone mass: Contribution of common genetic variation to extreme BMD phenotypes and potential novel BMD-associated genes. Bone. 2018;114:62-71.

12. Gregson CL, Sayers A, Lazar V, Steel S, Dennison EM, Cooper C, et al. The high bone mass phenotype is characterised by a combined cortical and trabecular bone phenotype: Findings from a pQCT case–control study. Bone. 2013;52(1):380-8.

13. Duncan EL, Danoy P, Kemp JP, Leo PJ, McCloskey E, Nicholson GC, et al. Genome-Wide Association Study Using Extreme Truncate Selection Identifies Novel Genes Affecting Bone Mineral Density and Fracture Risk. PLoS Genet. 2011;7(4):e1001372.

14. McInerney-Leo AM, Schmidts M, Cortes CR, Leo PJ, Gener B, Courtney AD, et al. Short-rib polydactyly and Jeune syndromes are caused by mutations in WDR60. Am J Hum Genet. 2013;93(3):515-23.

15. Adzhubei IA, Schmidt S, Peshkin L, Ramensky VE, Gerasimova A, Bork P, et al. A method and server for predicting damaging missense mutations. Nat Meth. 2010;7(4):248-9.

16. Kumar P, Henikoff S, Ng PC. Predicting the effects of coding non-synonymous variants on protein function using the SIFT algorithm. Nat Protoc. 2009;4(7):1073-81.

17. Morris JA, Kemp JP, Youlten SE, Laurent L, Logan JG, Chai RC, et al. An atlas of genetic influences on osteoporosis in humans and mice. Nature Genetics. 2019;51:258-66.

18. de Leeuw CA, Mooij JM, Heskes T, Posthuma D. MAGMA: generalized gene-set analysis of GWAS data. PLoS computational biology. 2015;11(4):e1004219.

19. Watanabe K, Stringer S, Frei O, Mirkov MU, Polderman TJC, van der Sluis S, et al. A global overview of pleiotropy and genetic architecture in complex traits. 2018:500090.

20. Hart T, Komori HK, LaMere S, Podshivalova K, Salomon DR. Finding the active genes in deep RNA-seq gene expression studies. BMC Genomics. 2013;14:778.

21. Youlten S, Baldock P, Leitch V, Quinn J, Bartonicek N, Chai R, et al. Osteocytes express a unique transcriptome that underpins skeletal homeostasis. American Society for Bone and Mineral Research; Denver, Colarado: http://www.asbmr.org/education/2017-abstracts; 2017.

22. Ferrer-Costa C, Gelpí JL, Zamakola L, Parraga I, de la Cruz X, Orozco M. PMUT: a web-based tool for the annotation of pathological mutations on proteins. Bioinformatics. 2005;21(14):3176-8.

23. Schwarz JM, Rodelsperger C, Schuelke M, Seelow D. MutationTaster evaluates disease-causing potential of sequence alterations. Nat Meth. 2010;7(8):575-6.

24. Zimmermann L, Stephens A, Nam SZ, Rau D, Kubler J, Lozajic M, et al. A Completely Reimplemented MPI Bioinformatics Toolkit with a New HHpred Server at its Core. J Mol Biol. 2018;430(15):2237-43.

25. Webb B, Sali A. Comparative Protein Structure Modeling Using MODELLER. Current protocols in bioinformatics. 2016;54:5.6.1-5.6.37.

26. Pettersen EF, Goddard TD, Huang CC, Couch GS, Greenblatt DM, Meng EC, et al. UCSF Chimera--a visualization system for exploratory research and analysis. Journal of computational chemistry. 2004;25(13):1605-12.

27. Alexander C, Zuniga E, Blitz IL, Wada N, Le Pabic P, Javidan Y, et al. Combinatorial roles for BMPs and Endothelin 1 in patterning the dorsal-ventral axis of the craniofacial skeleton. Development (Cambridge, England). 2011;138(23):5135-46.

28. Spoorendonk KM, Peterson-Maduro J, Renn J, Trowe T, Kranenbarg S, Winkler C, et al. Retinoic acid and Cyp26b1 are critical regulators of osteogenesis in the axial skeleton. 2008;135(22):3765-74.

29. Westerfield M. The zebrafish book. A guide for the laboratory use of zebrafish (Danio rerio).2000.

30. Bergen DJM, Stevenson NL, Skinner REH, Stephens DJ, Hammond CL. The Golgi matrix protein giantin is required for normal cilia function in zebrafish. 2017:bio.025502.

31. Hammond CL, Schulte-Merker S. Two populations of endochondral osteoblasts with differential sensitivity to Hedgehog signalling. Development (Cambridge, England). 2009;136(23):3991-4000.

32. Schindelin J, Arganda-Carreras I, Frise E, Kaynig V, Longair M, Pietzsch T, et al. Fiji: an open-source platform for biological-image analysis. Nature methods. 2012;9(7):676-82.

33. Zheng HF, Forgetta V, Hsu YH, Estrada K, Rosello-Diez A, Leo PJ, et al. Whole-genome sequencing identifies EN1 as a determinant of bone density and fracture. Nature. 2015;526(7571):112-7.

34. Stitziel NO, Stirrups KE, Masca NG, Erdmann J, Ferrario PG, Konig IR, et al. Coding Variation in ANGPTL4, LPL, and SVEP1 and the Risk of Coronary Disease. N Engl J Med. 2016;374(12):1134-44.

35. Webb TR, Erdmann J, Stirrups KE, Stitziel NO, Masca NG, Jansen H, et al. Systematic Evaluation of Pleiotropy Identifies 6 Further Loci Associated With Coronary Artery Disease. J Am Coll Cardiol. 2017;69(7):823-36.

36. Nelson CP, Goel A, Butterworth AS, Kanoni S, Webb TR, Marouli E, et al. Association analyses based on false discovery rate implicate new loci for coronary artery disease. Nat Genet. 2017;49(9):1385-91.

37. Dallas SL, Bonewald LF. Dynamics of the transition from osteoblast to osteocyte. Ann N Y Acad Sci. 2010;1192:437-43.

38. Bergen DJM, Kague E, Hammond CL. Zebrafish as an Emerging Model for Osteoporosis: A Primary Testing Platform for Screening New Osteo-Active Compounds. 2019;10(6).

39. Tsukamoto S, Mizuta T, Fujimoto M, Ohte S, Osawa K, Miyamoto A, et al. Smad9 is a new type of transcriptional regulator in bone morphogenetic protein signaling. Sci Rep. 2014;4:7596.

40. Butler WT, Mikulski A, Urist MR, Bridges G, Uyeno S. Noncollagenous proteins of a rat dentin matrix possessing bone morphogenetic activity. Journal of dental research. 1977;56(3):228-32.

41. Lowery JW, Rosen V. The BMP Pathway and Its Inhibitors in the Skeleton. Physiol Rev. 2018;98(4):2431-52.

42. Huang Z, Wang D, Ihida-Stansbury K, Jones PL, Martin JF. Defective pulmonary vascular remodeling in Smad8 mutant mice. Human Molecular Genetics. 2009;18(15):2791-801.

43. Arnold SJ, Maretto S, Islam A, Bikoff EK, Robertson EJ. Dose-dependent Smad1, Smad5 and Smad8 signaling in the early mouse embryo. Dev Biol. 2006;296(1):104-18.

44. Kemp JP, Morris JA, Medina-Gomez C, Forgetta V, Warrington NM, Youlten SE, et al. Identification of 153 new loci associated with heel bone mineral density and functional involvement of GPC6 in osteoporosis. Nat Genet. 2017;49(10):1468-75.

45. Medina-Gomez C, Kemp JP, Trajanoska K, Luan J, Chesi A, Ahluwalia TS, et al. Life-Course Genome-wide Association Study Meta-analysis of Total Body BMD and Assessment of Age-Specific Effects. Am J Hum Genet. 2018;102(1):88-102.

46. Koay MA, Woon PY, Zhang Y, Miles LJ, Duncan EL, Ralston SH, et al. Influence of LRP5 Polymorphisms on Normal Variation in BMD. J Bone Miner Res. 2004;19(10):1619-27.

47. Uitterlinden AG, Arp PP, Paeper BW, Charmley P, Proll S, Rivadeneira F, et al. Polymorphisms in the sclerosteosis/van Buchem disease gene (SOST) region are associated with bone-mineral density in elderly whites. Am J Hum Genet. 2004;75(6):1032-45.

48. Boyden LM, Mao J, Belsky J, Mitzner L, Farhi A, Mitnick MA, et al. High bone density due to a mutation in LDL-receptor-related protein 5. New Eng J Med. 2002;346(20):1513-21.

49. Hamersma H, Gardner J, Beighton P. The natural history of sclerosteosis. Clinical Genetics. 2003;63(3):192-7.

50. Xiao J, Purcell SA, Prado CM, Gonzalez MC. Fat mass to fat-free mass ratio reference values from NHANES III using bioelectrical impedance analysis. Clinical Nutrition. 2018;37(6, Part A):2284-7.

51. Frost M, Andersen T, Gossiel F, Hansen S, Bollerslev J, Van Hul W, et al. Levels of serotonin, sclerostin, bone turnover markers as well as bone density and microarchitecture in patients with high bone mass phenotype due to a mutation in Lrp5. J Bone Miner Res. 2011;26(8):1721-8.

52. Gregson CL, Poole KES, McCloskey EV, Duncan EL, Rittweger J, Fraser WD, et al. Elevated Circulating Sclerostin Concentrations in Individuals With High Bone Mass, With and Without LRP5 Mutations. J Clin Endocrinol Metab. 2014;99(8):2897-907.

53. Bonewald L. Use it or lose it to age: A review of bone and muscle communication. Bone. 2018;120:212-8.

54. Tosca L, Brisset S, Petit FM, Metay C, Latour S, Lautier B, et al. Genotype-phenotype correlation in 13q13.3-q21.3 deletion. European journal of medical genetics. 2011;54(5):e489-94.

55. Shintani M, Yagi H, Nakayama T, Saji T, Matsuoka R. A new nonsense mutation of SMAD8 associated with pulmonary arterial hypertension. J Med Genet. 2009;46(5):331-7.

56. Drake KM, Zygmunt D, Mavrakis L, Harbor P, Wang L, Comhair SA, et al. Altered MicroRNA processing in heritable pulmonary arterial hypertension: an important role for Smad-8. American journal of respiratory and critical care medicine. 2011;184(12):1400-8.

57. Walcott BP, Winkler EA, Zhou S, Birk H, Guo D, Koch MJ, et al. Identification of a rare BMP pathway mutation in a non-syndromic human brain arteriovenous malformation via exome sequencing. Human Genome Variation. 2018;5:18001.

58. Ngeow J, Yu W, Yehia L, Niazi F, Chen J, Tang X, et al. Exome Sequencing Reveals Germline SMAD9 Mutation That Reduces Phosphatase and Tensin Homolog Expression and Is Associated With Hamartomatous Polyposis and Gastrointestinal Ganglioneuromas. Gastroenterology. 2015;149(4):886-9.e5.

59. Le Goff C, Mahaut C, Wang Lauren W, Allali S, Abhyankar A, Jensen S, et al. Mutations in the TGFβ Binding-Protein-Like Domain 5 of FBN1 Are Responsible for Acromicric and Geleophysic Dysplasias. The American Journal of Human Genetics. 2011;89(1):7-14.

60. Loeys BL, Gerber EE, Riegert-Johnson D, Iqbal S, Whiteman P, McConnell V, et al. Mutations in fibrillin-1 cause congenital scleroderma: stiff skin syndrome. Science translational medicine. 2010;2(23):23ra0.

61. Rommel K, Karck M, Haverich A, von Kodolitsch Y, Rybczynski M, Muller G, et al. Identification of 29 novel and nine recurrent fibrillin-1 (FBN1) mutations and genotype-phenotype correlations in 76 patients with Marfan syndrome. Hum Mutat. 2005;26(6):529-39.

62. Timberlake AT, Choi J, Zaidi S, Lu Q, Nelson-Williams C, Brooks ED, et al. Two locus inheritance of non-syndromic midline craniosynostosis via rare SMAD6 and common BMP2 alleles. eLife. 2016;5.

63. Shore EM, Xu M, Feldman GJ, Fenstermacher DA, Cho TJ, Choi IH, et al. A recurrent mutation in the BMP type I receptor ACVR1 causes inherited and sporadic fibrodysplasia ossificans progressiva. Nat Genet. 2006;38(5):525-7.

64. Barruet E, Morales BM, Cain CJ, Ton AN, Wentworth KL, Chan TV, et al. NF-κB/MAPK activation underlies ACVR1-mediated inflammation in human heterotopic ossification. JCI insight. 2018;3(22):e122958.

65. Sheu TJ, Zhou W, Fan J, Zhou H, Zuscik MJ, Xie C, et al. Decreased BMP2 signal in GIT1 knockout mice slows bone healing. 2014;397(1):67-74.

66. Hankenson KD, Gagne K, Shaughnessy M. Extracellular signaling molecules to promote fracture healing and bone regeneration. Advanced drug delivery reviews. 2015;94:3-12.

67. Salazar VS, Gamer LW, Rosen V. BMP signalling in skeletal development, disease and repair. Nat Rev Endocrinol. 2016;12(4):203-21.

68. Duncan EL, Cardon LR, Sinsheimer JS, Wass JA, Brown MA. Site and gender specificity of inheritance of bone mineral density. J Bone Miner Res. 2003;18(8):1531-8.

Figure Legends

Fig 1: The HBM pedigree and electrophoretogram images of a segregating *SMAD9* c.65T>C, p.Leu22Pro variant

Fig 2: GWAS for eBMD measured in UK Biobank: Regional association plot for the locus containing *SMAD9*. Top panel: circles show unconditioned GWAS *P*-values and genomic locations of imputed SNPs within +/- 800kb of the 5' and 3' UTR of each gene. Colours indicate varying degrees of pairwise linkage disequilibrium between the lead eBMD-associated SNP (rs12427846, purple diamond) and all other SNPs. Second panel: Vertical shaded areas correspond to locations of DNase I hypersensitive sites (DHSs) characteristic of: skeletal muscle myoblasts cell line (E120), osteoblast primary cells (E129), mesenchymal stem cell derived chondrocyte cultured cells (E049) and mesenchymal stem cell derived adipocyte cultured cells (E023). Red shading depicts intersections between DHSs and genome-wide significant SNPs. Black shading denotes instances in which any other SNPs intersect DHSs. Third panel: Blue circle shows the position of the putative causal variant c.65T>C, p.Leu22Pro. Fifth panel: Horizontal lines represent genes with vertical lines annotating location of exons. Arrows indicate the direction in which each gene is transcribed.

Fig 3: Smad9 protein expression in the larval zebrafish opercle bone

A. Schematic of the larval zebrafish head (6 days post fertilisation (dpf), lateral view), showing visible ossified elements (red) and the main muscle groups (green) that are green fluorescent protein (GFP) positive under control of the BMP responsive elements promoter (BMPre) transgenic reporter line (*BMPre:GFP*). The black box indicates the location of the intramembranous opercle bone as shown in panels B and C. ***B. Distinct tissue distribution of***

Smad9- and BMP-expressing cells (7dpf). Upper left panel: *BMPre:GFP* positive cells (white) in the levator operculi muscle group (white arrow) and ventral (V) side of the opercle (OP; dotted blue outline); upper middle: distinct group of Smad9 positive cells (white) in the dorsal (D) tip of the opercle; upper right: merged view showing distinct tissue expression of *BMPre:GFP* positive cells (green) and Smad9 positive cells (purple); lower left: grey box inset (i) showing faint cap of *BMPre:GFP* positive cells at the dorsal tip of the opercle (red arrow); lower middle: cluster of Smad9 positive cells; lower right: merged view confirming non-overlapping distribution of *BMPre:GFP* positive cells and Smad9 positive cells. Images from n=4 larvae. ***C. Distinct tissue distribution of Smad9- and osterix (Sp7)-expressing cells*** (6dpf). Upper left: *Sp7:GFP*-positive osteoblasts (OB; white) within the opercle; upper middle: Smad9 positive cells (white) in the antero (A)-dorsal tip of the opercle (red arrow); upper right: merged view showing separation of *Sp7:GFP* positive cells (green) and Smad9 positive cells (purple) (Supplemental Movie 1); lower left: the inset (i, grey box) shows few *Sp7:GFP*-positive osteoblasts within the dorsal tip of the opercle; lower middle: cluster of Smad9 positive cells; lower right: merged view confirming non-overlapping distribution of *Sp7:GFP* and Smad9 positive cells. Images from n=6 larvae. B and C: scale bar =20 μm; all are maximum intensity z-projection confocal images. Abbreviations: A, anterior; BR, branchiostegal ray; CL, cleithrum; D, dorsal; M, muscle; MC, Meckel's cartilage; MX, maxilla; OB, osteoblast; OP, operculum; P, posterior; V, ventral.

Fig 4: Figure illustrating position of c.65T>C p.Leu22Pro variant within *SMAD9*

Fig 5: (A) Wildtype (WT) *SMAD9* MH1 domain (light green ribbon with helix-1 in light blue) binding the DNA helix (dark blue/dark green). L22 is shown in blue space-filling.

(B) L22P, shown in red space-filling, is predicted to severely disrupt the structure of the MH1 domain. Supplemental Movie 2: 3-dimensional rotating image

Table 1: Characteristics of the c.65T>C, p.Leu22Pro SMAD9 HBM pedigree members and two further unrelated HBM individuals with the same SMAD9 mutation

	HBM Pedigree					Additional Isolated HBM cases	
	UK proband III.1	UK half sister III.2	UK mother II.2	UK grand-mother I.2 (unaffected)		UK case	Australian case
SMAD9 Mutation	Leu22Pro	Leu22Pro	Leu22Pro	WT		Leu22Pro	Leu22Pro
Age at assessment	33	22	55	75		55	57
Sex	Female	Female	Female	Female		Female	Female
Ethnicity	Caucasian	Caucasian	Caucasian	Caucasian		Caucasian	Caucasian
Anthropometry							
Height (cm)	178.0	173.3	175.0	160.6		160.0	162.2
Weight (kg)	138.0	133.8	127.8	72.6		89.7	69.9
BMI (kg/m^2)	43.6	43.3	41.4	28.1		35.0	26.6
DXA Measurements							
Total Hip BMD Z-score	+3.2	+4.8	+3.3	+0.1		+4.3	+2.7
L1 BMD Z-score	+4.5	+2.6	+3.3	+0.8		+5.0	+3.4*
BMC (kg)	3.49	3.77	3.65	2.12		3.24	-
Fat mass (kg)	73.2	64.5	64.8	25.4		34.0	-
Lean mass (kg)	61.3	65.6	59.5	45		52.4	-
Clinical phenotype							
Adult Fracture	No	No	No	No		No	No
Sinks/ Floats	Floats	Sinks	Floats	Floats		Sinks	-
Bone pain	Yes	Yes	Yes	No		No	-
Visual/auditory impairment	Myopia	No	No	Impaired hearing		Astigmatism	-
Dentition	Normal	Normal	Normal	Normal		Retained cuspid tooth	-
Shoe Size [a]	10	10	9	6		5.5	-
Broad Frame	Yes	Yes	Yes	No		Yes	-
Enlarged Mandible	Yes	Yes	Yes	No		Yes	-
Torus	Yes	Yes	No	No		No	-
Nerve compression	No	No	No	No		No	-
Pes planus	No	No	Yes	No		Yes	-
Blood tests							
ALP (IU/L)	99	83	102	202		61	-
Adjusted calcium (mmol/L)	2.50	2.46	2.40	2.46		2.33	-
P1NP (ug/L)	58	36	22	95		35	-
CTX (ug/L)	0.15	0.18	0.19	0.10		0.16	-
Osteocalcin (ug/L)	12.4	17.1	13.5	14.8		11.5	-
Sclerostin (pmol/L)	71.0	-	56.1	44.4		50.4	-

WT: Wild type. [a] UK measurements. Reference ranges; ALP 20-120, Adjusted calcium 2.25-2.70, P1NP: pre-menopausal 30-78 ug/L, postmenopausal 26-110 ug/L, male 20-76 ug/L. Serum CTX 0.1-0.5ug/L, Osteocalcin 6.8-32.2ug/L. Sclerostin <80 pmol/L.

Table 2: Distal and mid-shaft tibial pQCT measures in High Bone Mass cases compared with female HBM cases without SMAD9, LRP5, LRP4, SOST mutations, and female family controls with normal BMD

		SMAD9 HBM cases Leu22Pro n=4 Mean (SD)	WT Female HBM cases[1] n=76 Mean (SD)	p value[2]	Female family controls with normal BMD n=32 Mean (SD)	p value[3]
	Age (years)	41.3 (16.5)	60.8 (12.3)		54.8 (13.5)	
	Total Hip BMD Z-Score	+3.8	+2.9		+0.39	
4% Distal Tibia	Total Bone area (mm^2)	1038 (160.6)	1052 (122.6)	0.820	817.1 (223.5)	0.066
	Trabecular BMD (mg/cm^3)	342.3 (13.3)	324.3 (22.5)	0.118	308.0 (24.6)	0.010
	Cortical thickness (mm)	2.12 (0.79)	1.04 (0.81)	0.011	0.87 (0.83)	0.007
66% Mid-shaft Tibia[4]	Total Bone area (mm^2)	608.3 (4.7)	601.5 (81.9)	0.886	572.7 (73.9)	0.416
	Cortical BMD (mg/cm^3)	1150 (10.1)	1126 (35.9)	0.255	1111 (65.7)	0.319
	Cortical thickness (mm)	4.96 (0.13)	4.37 (0.62)	0.104	3.80 (0.71)	0.008
	Cortical Bone Area (mm^2)	356.3 (9.1)	316.6 (36.6)	0.065	274.1 (42.4)	0.002
	Cortical/Total Bone area (%)	58.6 (1.1)	53.3 (7.57)	0.236	48.3 (8.34)	0.043
	SSI (mm^3)	1680 (21.1)	1506 (236.6)	0.211	1298 (248.2)	0.013
	Muscle area (mm^2)	8334 (536.5)	6939 (980.8)	0.017	6542 (1033)	0.006
	Muscle density (mg/cm^3)	42.1 (1.5)	40.1 (4.0)	0.392	40.2 (3.1)	0.323

HBM: High Bone Mass, BMD: Bone Mineral Density, SD: Standard Deviation, SSI: Strength Strain Index, WT: Wildtype.

[1] Female subgroup (without *SMAD9, LRP5, LRP4, SOST* mutations) analysed using data previously published, collected and analysed with the same protocols as *SMAD9* HBM cases (9). Analysis of *SMAD9* HBM cases vs. WT HBM cases[2] and Family controls with normal BMD[3]. [4] n=3